

Comparison of gully erosion estimates using airborne and ground-based LiDAR on Santa Cruz Island, California

Ryan L. Perroy ^{a,*}, Bodo Bookhagen ^b, Gregory P. Asner ^c, Oliver A. Chadwick ^b

^a Department of Geography and Earth Science, University of Wisconsin-La Crosse, 1725 State Street, La Crosse, WI 54601, USA

^b Department of Geography, 1832 Ellison Hall, UC Santa Barbara, Santa Barbara, CA 93106-4060, USA

^c Department of Global Ecology, Carnegie Institution, 260 Panama Street, Stanford, CA 94305, USA

ARTICLE INFO

Article history:

Received 11 October 2009

Received in revised form 9 January 2010

Accepted 14 January 2010

Available online 22 January 2010

Keywords:

Erosion

Gully

LiDAR

Volume estimates

Mediterranean climate

ABSTRACT

Gully erosion removes comparatively large volumes of soil from small areas. It is often difficult to quantify the loss of soil because the footprint of individual gullies is too small to be captured by most generally available digital elevation models (DEMs), such as the USGS National Elevation Dataset. Airborne LiDAR (Light Detection and Ranging) has the potential to provide the required data density, but an even newer class of ground-based sensors may provide better local resolution at lower cost. In this study, we compared digital elevation models produced by airborne and ground-based LiDAR systems with ground-based geomorphic and geodetic survey data to determine their utility in quantifying volumetric soil loss due to gully erosion in a heavily degraded watershed ($7.55 \times 10^{-2} \text{ km}^2$), on southwestern Santa Cruz Island in southern California. Volumetric estimates of the eroded sediment were produced by comparing the LiDAR-derived DEMs of the gully system to a modeled pre-erosion surface. Average point densities were significantly higher for the ground-based LiDAR system and provided more detailed information; however, its limited scanning footprint and side-looking orientation presented serious challenges in collecting continuous data from deeply incised gullies, making the airborne system preferable for this type of investigation and likely for most applications where heavy topographic shadowing is prevalent.

© 2010 Elsevier B.V. All rights reserved.

1. Introduction

Gully erosion, the removal of soil from narrow channels via the accumulation of surface runoff, tends to produce more sediment loss than other forms of soil erosion such as overland flow or rilling (Wasson et al., 2002; Poesen et al., 2003; De Vente et al., 2005; Huon et al., 2005; Wells et al., 2009). Gullies are generally defined by their channel depth, which for permanent gullies can range from 0.5 to 30 m (Soil Science Society of America, 2001). They are also one of the most destructive forms of erosion, destroying soil, undermining infrastructure, damaging agricultural fields, altering transportation corridors, and lowering water tables (Valentin et al., 2005). Furthermore, their damage is difficult to reverse. Gully erosion dramatically affects sediment budgets and flux rates, and influences stream dynamics as evidenced from data on hydrographs (Kelsey, 1980; Costa and Bacellar, 2007). In addition, in some areas gully erosion is directly linked to changing climatic conditions (Nearing et al., 2004; Chaplot et al., 2005; Nunes et al., 2008, 2009). Quantifying gully erosion will assist in understanding gully formation and spatiotemporal evolution. Although gullies are visually striking, their small spatial extent generally renders them undetectable in most generally available topographic datasets. The goal of this work was to test the viability of

applying airborne and ground-based LiDAR technology to quantify gully erosion on southwestern Santa Cruz Island in southern California. Limited by the minimum spot spacing of the airborne LiDAR dataset, our study only considered gullies with a width of >2 m.

Previous attempts to quantify gully erosion have usually involved labor-intensive field measurements, such as field tapes, micro profilers, theodolite or total station, and differential GPS methods (Lawler, 1993; Casalí et al., 2006; Moody and Kinner, 2006; Nyssen et al., 2006; Rustomji, 2006; Wu et al., 2008). Erosion pins have also been used to measure gully wall retreat (Ireland et al., 1939; Brumbaugh, 1983). In addition to being spatially limited in scope, these methods are all time consuming, tedious, labor intensive, and expensive. By contrast, high-resolution LiDAR datasets offer the potential to efficiently measure gully volumes at the landscape scale. Until recently, the resolution of available topographic digital elevation models (DEMs) (National Elevation Dataset, USGS topographic maps, Shuttle Radar Topographic Mission), has not been fine enough to capture small features such as gullies. An exception are DEMs produced via digital photogrammetric analysis, which have allowed measurements of gully-scale erosion (Betts and DeRose, 1999; Martinez-Casanovas, 2003; Martinez-Casanovas et al., 2004). Recent work on three-dimensional gully monitoring using low altitude, unmanned platforms has produced extremely high-resolution (5 and 7.5 cm pixel size) DEMs (Marzolff and Poesen, 2009). Although photogrammetry has made impressive advances in the past few years, the growing proliferation

* Corresponding author. Tel.: +1 608 785 8334; fax: +1 608 785 8332.

E-mail address: perroy.ryan@uwlax.edu (R.L. Perroy).

and availability of LiDAR datasets and increasing number of recent LiDAR-derived morphometric studies highlight the potential of this technology to quantify and monitor gully erosion. Though the majority of high-resolution LiDAR studies have been associated with fluvial systems (e.g., Thoma et al., 2005; Heritage and Hetherington, 2007; Milan et al., 2007), the widening geomorphic applications include landsliding (McKean and Roering, 2004; Glenn et al., 2006), seasonal hillslope erosion rates (Wawrzyniec et al., 2007), and coastal cliff erosion (Rosser et al., 2005; Young and Ashford, 2006).

There have been very few studies specifically applying LiDAR technology to gully erosion, and these have focused exclusively on either airborne or ground-based instruments. In two studies using ground-based systems, Hancock et al. (2008) examined incipient rill and gully formation on mine spoils, while Collins and Kayen (2006) and Collins et al. (2008, 2009) mapped gully thalwegs and geomorphic changes associated with sensitive archeological sites in Grand Canyon National Park. In the first of two existing gully studies using airborne LiDAR data, James et al. (2007) attempted to map gullies and headwater streams under dense forest canopy in the southeastern United States with limited success. In the second study, most relevant to the present work, Eustace et al. (2009) used a semi-automated object oriented classification method to detect and map gully extent and volume in eastern Australia. Although this method yielded impressive mapping results when compared to high-resolution Quickbird satellite imagery, no field data were gathered to verify the volumetric gully estimates. This present study directly compares gully volume estimates produced by ground-based and airborne LiDAR systems to data collected in the field, with the goal of assessing the utility of the two systems for measuring gully volumes at a landscape scale.

This study follows three steps to compare gully erosion estimates produced by two different LiDAR systems (airborne and ground based) over a $<0.1 \text{ km}^2$ catchment: (1) raw LiDAR point cloud data were collected and processed to produce bare-earth DEMs. (2) DEM accuracy was assessed by comparison with total station and differential GPS data

collected in the field. (3) A 'pre-erosion' surface was modeled by removing gully features from the existing DEMs, and the difference between the present-day and pre-erosion surfaces was calculated to produce a volumetric gully erosion estimate.

2. Regional setting

Santa Cruz Island (SCI), the largest of the California Channel Islands, is located 38 km off the central California coast (Fig. 1). The island is roughly 37 km long east to west and ranges from 3 to 11 km wide, north to south. An unsustainable increase in the sheep population during the late 19th century led to widespread vegetation denudation and erosion across the island, most notably in Pozo canyon in the southwest (Junak et al., 1995). Based on a combination of historic and field evidence, widespread gullying in Pozo canyon was initiated between 1878 and 1886, largely stabilizing by 1929 (Perroy, 2009). A $7.55 \times 10^{-2} \text{ km}^2$ heavily gullied sub watershed of lower Pozo canyon (Fig. 1C, green box) was selected for this work. It is underlain by the Canada Formation, a weakly lithified micaceous clay shale that is part of a sequence of highly erosive Tertiary sedimentary units found on southwestern SCI. Soils in the study area are vertisols with extensive piping (Brumbaugh, 1983; Perroy, 2009).

3. Methods

3.1. Data collection

3.1.1. Airborne LiDAR

Airborne LiDAR data were collected over SCI using the Carnegie Airborne Observatory, an instrument fusing hyperspectral and waveform LiDAR data with a global positioning system-inertial measurement unit (GPS-IMU) (Asner et al., 2007, 2008). The instrument was flown at an altitude of 3000 m above ground level (agl) onboard a Twin Otter aircraft, resulting in a laser spot spacing of approximately 1.5 m. The

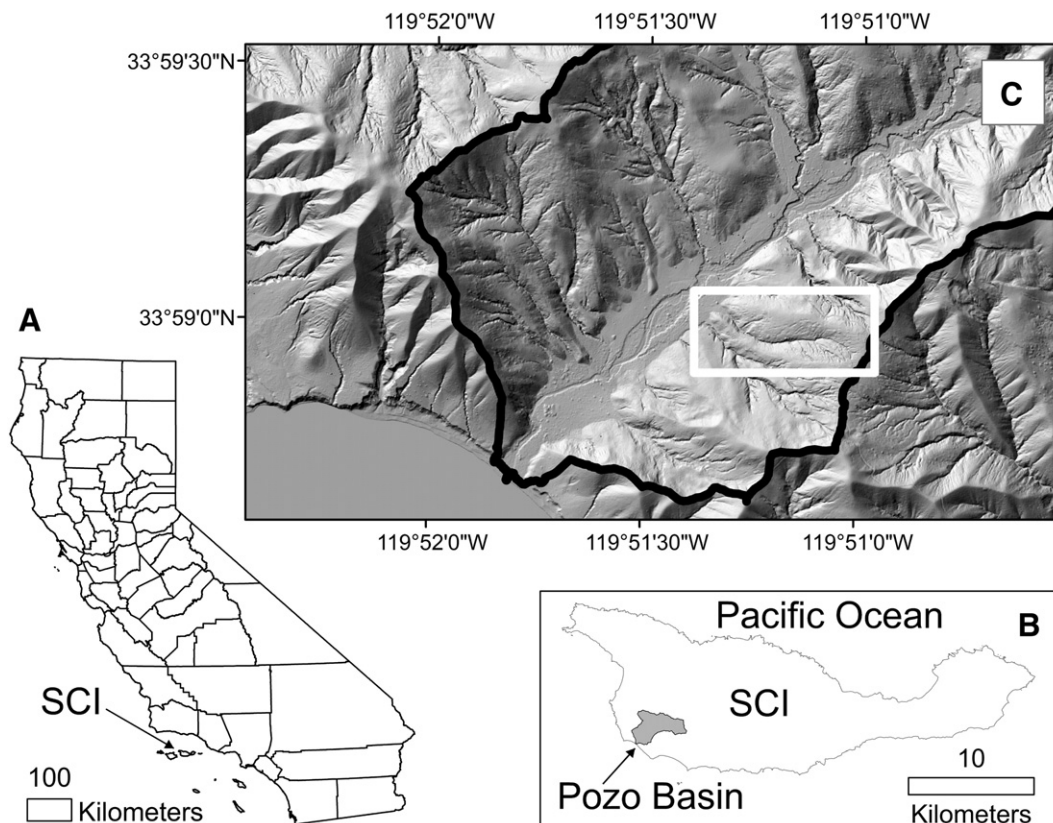
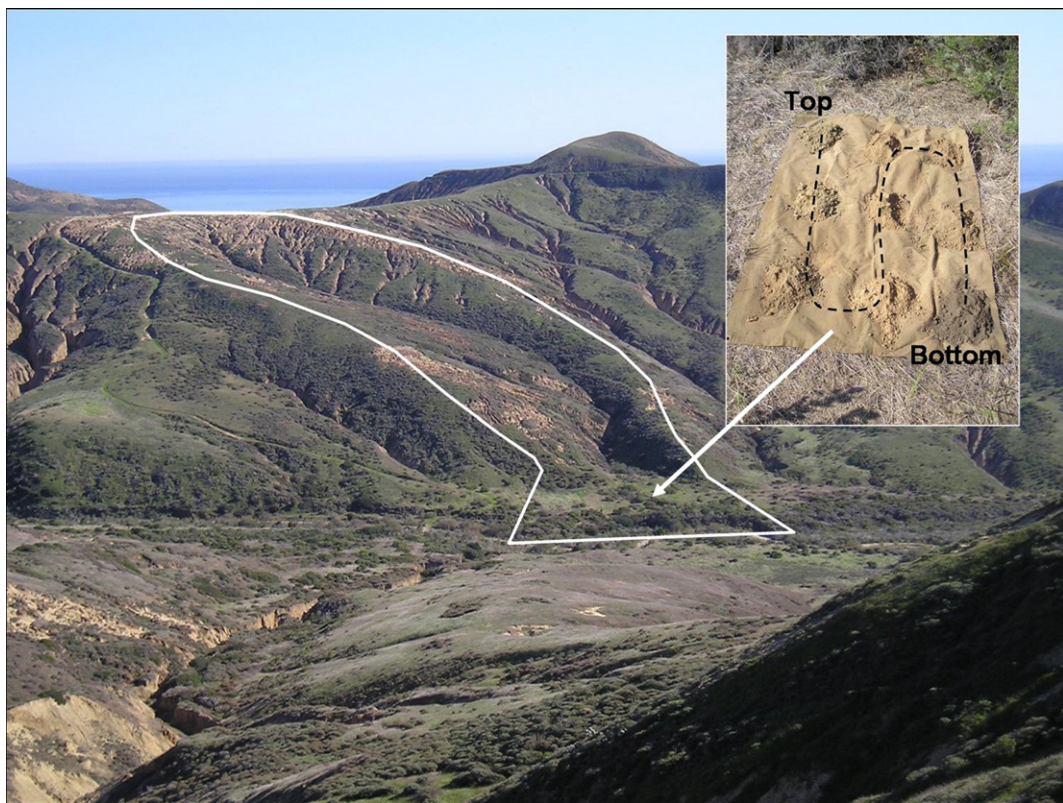
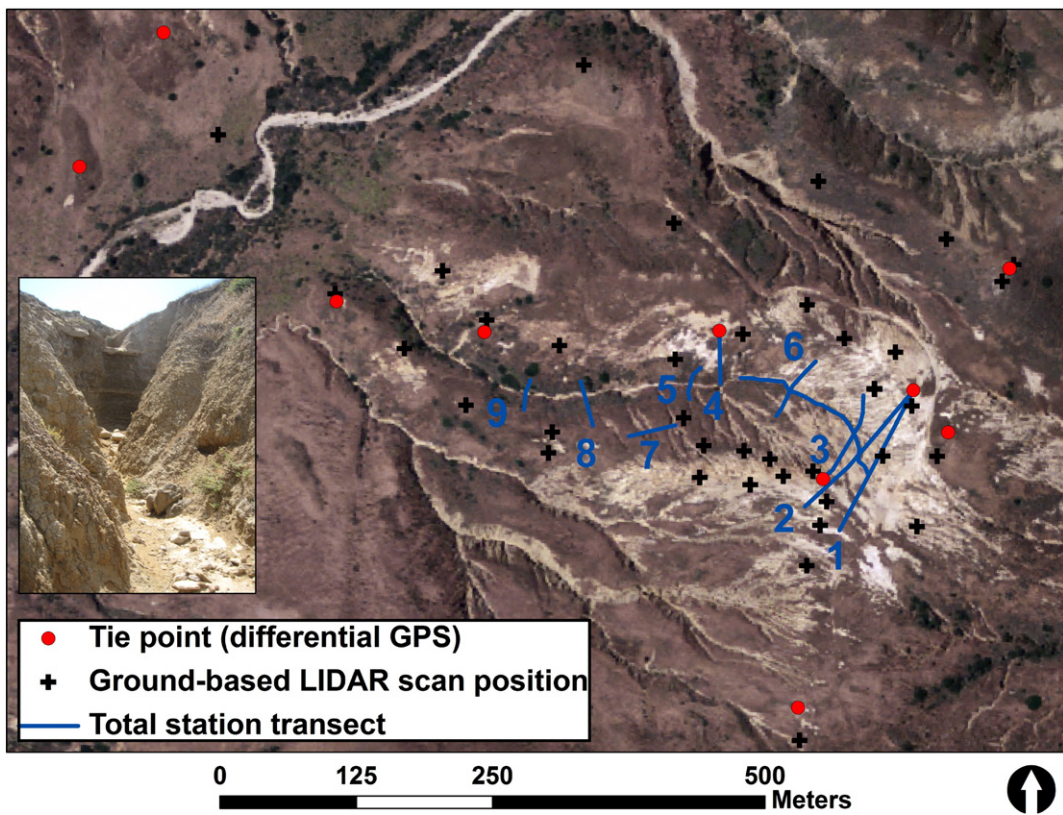


Fig. 1. Study area. A) Location of Santa Cruz Island (SCI) in California State. B) Pozo watershed, shaded in grey, on southwestern SCI. C) Airborne LiDAR hillshade-relief image of Lower Pozo basin showing extensive gullying. Study area tributary outlined in white.



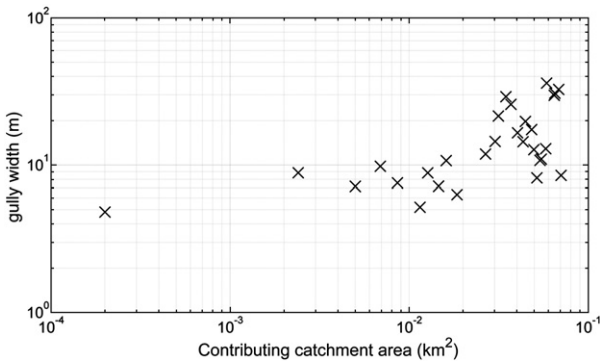


Fig. 4. Log-log plot of contributing catchment area (km^2) vs. gully width (m) for study site. Our data do not support a power-law relation between contributing area and gully width.

Carnegie Airborne Observatory can produce LiDAR datasets with much higher point densities, but the primary mission requirements of the Santa Cruz Island dataset (invasive vegetation species mapping) dictated a flight altitude that was higher than preferred for this application. The data were processed and precision corrected, producing a 1.5 m DEM.

As a first step, the GPS-IMU and LiDAR raw point data were combined to determine the location of the laser returns within three-dimensional space. A ground digital elevation model was then created from the orthorectified LiDAR point cloud using a physical model to estimate top-of-canopy and ground surfaces via REALM (Optech Inc., Vaughn, Canada) software and a custom macro script written for Terrascan/Terramatch (Terrasolid Ltd., Jyväskylä, Finland) for Microstation (Bentley Systems, Exton, PA). The basic macro steps involve:

1. Excluding erroneous points that are too high (e.g., bird strikes or vegetation) too low, or too isolated to be viable
2. Identifying ground points using an iterative classification process based on terrain angle, point distance, and return value within the waveform signal
3. Automatic and manual post processing to remove any falsely classified data points.

3.1.2. Ground-based LiDAR

Ground-based LiDAR data were collected in the field using a Riegl Model LMS-Z420i ground-based scanner (Horn, Austria). Data from 37 individual scan positions collected over three days were merged together using 29 common tiepoint reflectors, nine of them georeferenced using a Trimble L1/L2 differential GPS system with a base station within a 5-km range (Fig. 2). To register the nine GPS tiepoints, each point was measured for a minimum of 20 minutes and post processed using standard Trimble software. The registered LiDAR point cloud data were first processed using Riegl RiscanPro. Most notably, we reduced the 4.5×10^6 points per scan to a much smaller number by applying an octree filter with $25 \times 25 \times 1 \text{ cm}$ cubes (length \times width \times height). The octree filter segments the point cloud into cubes, reducing the data within each cube to a single point. This step allowed us to combine the point clouds from each scan into a single file. Next, we applied a custom macro script written for Terrascan/Terramatch (Terrasolid Ltd., Jyväskylä, Finland) for Microstation (Bentley Systems, Exton, PA) to produce a triangulated irregular network (TIN). We then converted the TIN into an equally spaced grid of 0.25 m horizontal resolution with a maximum vertical error of 0.05 m in order to use it for direct comparison to the airborne LiDAR.

3.1.3. Total station and GPS surveying

Total station survey measurements of the field site were collected for use as validation data. The total station data were georeferenced with the same tiepoints used in the ground-based LiDAR field campaign. Measurements of nine gully-cross sections were collected, ranging in width from 24.3 to 143.2 m, along with a topographic profile running along the axis of the main gully channel for a distance of 180 m (Fig. 2). Total station measurements were collected at centimeter-level resolution and specifically gathered to capture breaks in slope and other topographic features important for producing an accurate ground-surface survey. Individual clasts were ignored but data were collected on all other features larger than $\sim 10 \text{ cm}$. All together, 350 individual topographic datapoints were collected in the field. These data were used to assess the accuracy of the two LiDAR-derived DEMs.

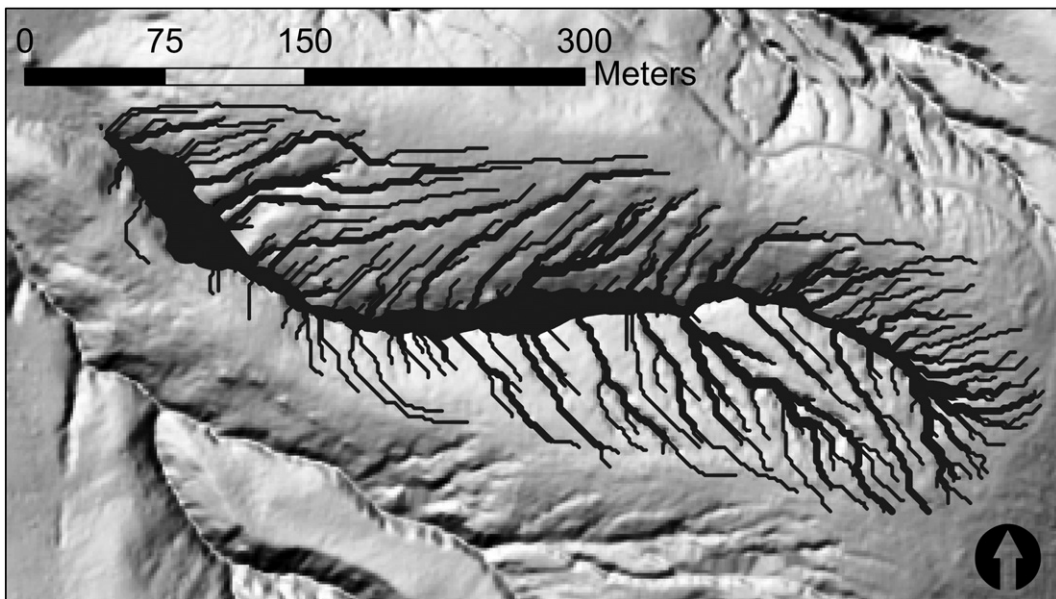


Fig. 5. Map of study area gully system showing GIS buffer used to identify gullied areas in study site. Buffer derived from a combination of differential GPS data, Horton–Strahler stream order for low-order gully tributaries, and hand digitizing. Area of buffer is 25,323.3 m^2 .

Differential GPS measurements were collected at 2-second intervals (approximately 2 m steps) while walking along the edges of four major gully channels, including the field site, to produce gully width measurements. These data were collected to map the boundary of the study site gully and to provide additional data for exploring the relation between gully width and contributing catchment area.

3.1.4. Volume estimation of sediment accumulation via hand-auger data

Hand-auger data were collected on the floodplain immediately below the study site to estimate the volume of sediment evacuated from the gully system and stored as alluvial fan deposits. Eighty-seven hand-auger holes were bored to measure the contact depth between pre-settlement floodplain soils and the recently deposited alluvial fan sediments. The contact boundary was identified by the strong contrast in color between the dark underlying floodplain soils (Munsell color 2.5 Y 5/2, dry) and the recently deposited alluvial fan sediments (Munsell color 2.5 Y 7/3, dry; Fig. 3). Depth to the boundary was measured with a tape measure and auger hole location mapped with either a referenced total station (accuracy ± 1.0 cm) or a handheld GPS unit (typical accuracy ± 3 m). Auger data were imported into a GIS program and interpolated using inverse-distance weighting to create an estimate of the alluvial fan volume.

3.2. Historic and recent aerial photography

Historic aerial photography was also used to understand the dynamics of the alluvial fan over time. Aerial photos from 1929, 1964 and 1989 were orthorectified using COSI-Corr, an open-source addition to the ENVI/IDL remote sensing software platform (Leprince et al., 2007; Ayoub et al., 2009). Imagery from the 2005 National Agriculture Imagery Program (NAIP) was used as the base image, with supporting topographic data from the 1.5 m LiDAR flight produced by the Carnegie Airborne Observatory. All orthorectified images were resampled to 1.5 m resolution. Registration error was calculated by selecting 10 points across the study site that were clearly identifiable in all four of the images (long-standing lone trees, road bends, incised gully junctions, etc.) and were not used in the original orthorectification processing steps. UTM coordinates for these 10 points were extracted from each image, and the difference from the 2005 NAIP image calculated. Maximum registration error was <10 m, which is within USGS National Map Accuracy Standards at the 1:12,000 scale and suitable for mapping the study site's highly dynamic alluvial fan activity.

3.3. Pre-erosion surface modeling

The 19th-century gullies in Pozo canyon eroded into a pre-existing landscape containing ephemeral tributaries and interfluves, and we reconstructed this pre-erosion surface as follows: (1) data points from the LiDAR point cloud that fell within the gully system were identified, (2) these points were removed from the point cloud, and (3) a DEM was created from the remaining 'non-gully' points using standard GIS grid-based linear interpolation techniques. This un-gullied surface was then compared to the present-day landscape to produce a volumetric estimate of the amount of sediment lost through gully incision. Although surface erosion via overland flow has undoubtedly occurred across the study area, we have focused on the gullies, specifically those with a width >2 m given the point spacing of the airborne LiDAR dataset, and do not take other forms of erosion into account. The intact soil profiles and deep A horizons of non-gullied locations within the study catchment suggest that sheet erosion is a relatively minor erosion factor in this landscape.

Multiple techniques were evaluated to identify gullies within the raw LiDAR data point cloud. A simple minimum slope threshold, commonly employed in standard LiDAR point-classification algorithms to isolate buildings or other landscape features with sharp angles in flat terrain (Vosselman and Maas, 2001), was unsuccessful in

identifying gully edges within the steeply sloping hillsides of the study site. A simple buffer technique, centered on gully channels with width scaled to Horton–Strahler stream order (Horton, 1945; Strahler, 1952), proved to be effective for the lowest order components of the gully system but failed at higher orders due to weak relationships between gully width and contributing catchment area in the study site (Fig. 4). Delineation of gullied and non-gullied data points was also accomplished within a GIS by incorporating gully width measurements collected via differential GPS in the field and hand digitizing.

The best means of delineating gullied vs. non-gullied areas for the study area was a combination of the differential GPS gully width

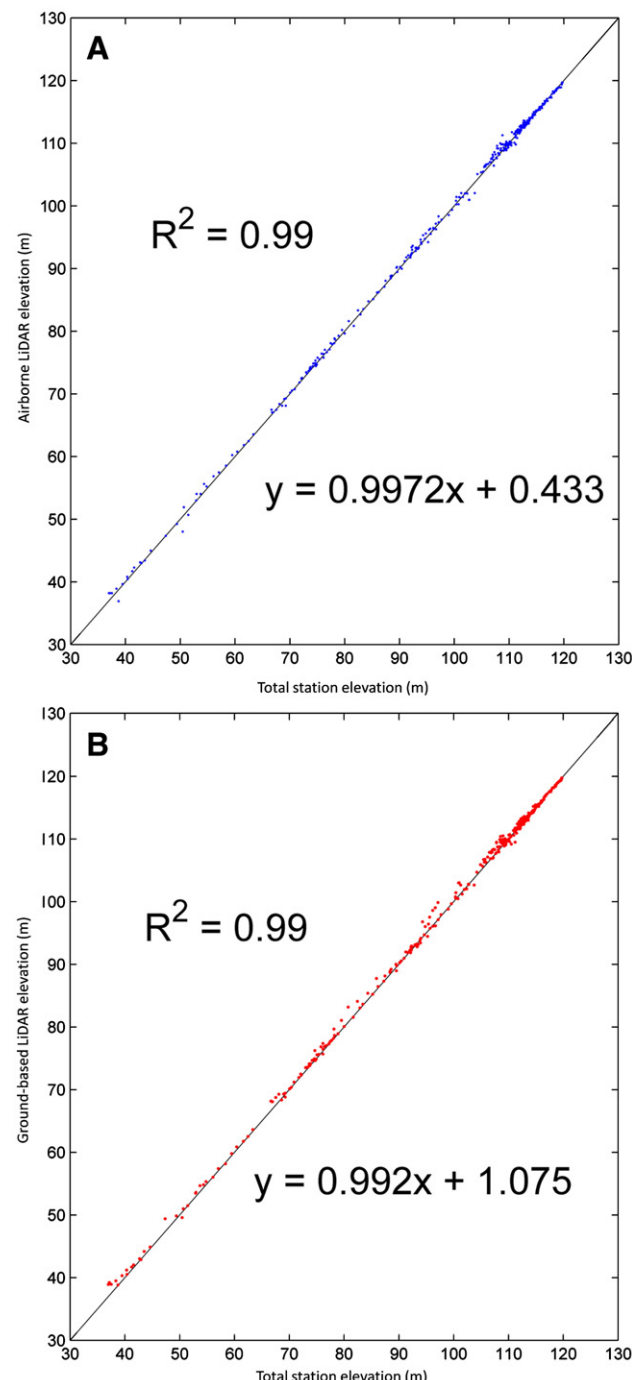


Fig. 6. Scatter plots of elevation from total station reference data and (A) airborne LiDAR and (B) ground-based LiDAR data for study site gully transects. Black line is 1:1 ratio. $n = 295$.

Table 1

Data for gully cross-sectional transects, as shown in Fig. 2.

Transect number	Transect length (m)	Total station cross-sectional area (m^2)	Airborne LiDAR cross-sectional area (m^2)	Ground-based LiDAR cross-sectional area (m^2)	Airborne LiDAR error (m^2 and %)	Ground-based LiDAR error (m^2 and %)
1	143	16,486	16,488	16,490	-2 (0.0)	-4 (0.0)
2	143	16,146	16,152	16,154	-6 (0.0)	-8 (0.0)
3	89	9648	9657	9658	-9 (-0.1)	-9 (-0.1)
4	47	3838	3836	3841	1 (0.0)	-3 (-0.1)
5	30	2164	2166	2175	-2 (-0.1)	-11 (-0.5)
6	63	5919	5920	5918	-1 (0.0)	1 (0.0)
7	47	3534	3543	3552	-9 (-0.3)	-18 (-0.5)
8	42	2292	2305	2310	-13 (-0.5)	-18 (-0.8)
9	24	985	991	1001	-6 (-0.6)	-16 (-1.6)

Errors are derived by comparing the cross-sectional areas for the total station and LiDAR datasets. Negative values indicate an underestimation of gully area; positive values indicate an overestimation.

measurements, a GIS buffer based upon Horton–Strahler stream order for low-order tributaries, and hand digitizing for higher-order tributaries (Fig. 5). Although not a fast, fully automated technique, these procedures provided the best results for the study area.

4. Results

4.1. Comparison of airborne and ground-based LiDAR with total station data

Spot elevations corresponding to the total station gully survey point locations were extracted from the two LiDAR-derived DEMs (Fig. 2). Overall agreement between both LiDAR datasets and total station data is excellent, with R^2 values of 0.99, though their regression equation offset values are different (0.43 for the airborne vs. 1.1 for the ground-based system) (Fig. 6). The gully transect data were then plotted and the cross-sectional area under each curve was numerically calculated. Gully estimation error was determined by the difference in cross-sectional area, with negative errors indicating an underestimation of gully depth and positive errors associated with an overestimation. Although both LiDAR systems generally underestimated gully depths and as a result, gully cross-sectional area, this was a larger problem for the ground-based system (Table 1). Example plots for transects #3, 5, and 6 are shown in Fig. 7.

4.2. LiDAR point density

LiDAR point density (the number of processed LiDAR data points present in a $1 m^2$ planimetric area) for both datasets was evaluated across the study area (Fig. 8, Table 2) and is also shown for the three transects in Fig. 7. Point densities for the extracted transect points ranged in value from 0 to 1.3 points m^{-2} for the airborne system and from 0 to 8.0 points m^{-2} for the ground-based system. Locations with low LiDAR point densities (black squares) and/or rapid changes in elevation often produced the largest errors.

A comparison of airborne and ground-based LiDAR elevation error histograms in Fig. 9 shows that both datasets are negatively skewed, meaning they are more likely to overestimate surface elevations (i.e. underestimate gully depth) than underestimate them. This is especially pertinent for estimating gully volumes, as overestimation of gully bottom elevation results in low erosion volumes and cross-sectional areas (Table 1). Fig. 10 shows a cumulative probability plot of absolute vertical errors for both the ground-based and airborne systems, segregated by gullied and un-gullied areas. For un-gullied area data (solid lines), the ground-based LiDAR consistently outperforms the airborne system, if only by a small amount. For the majority of gullied area data (broken lines), the ground-based system also either outperforms (below the marked black arrow) or does as well as the airborne

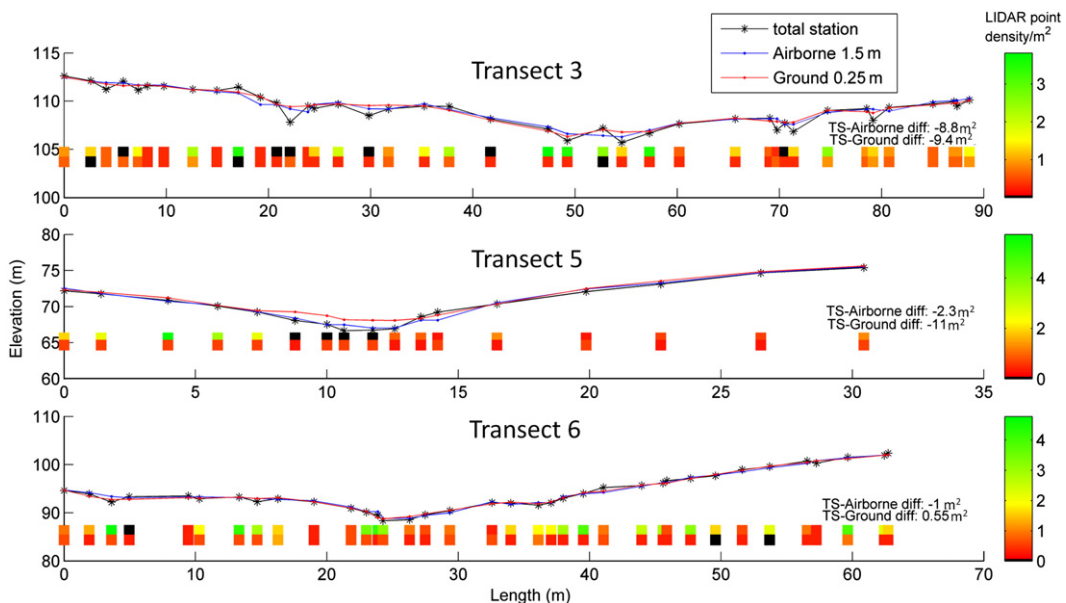


Fig. 7. Plots of three gully cross-sectional transects. Total station data shown in blue, airborne LiDAR data shown in green, ground-based LiDAR data shown in red. Calculated point density at total station point locations for the two LiDAR systems is depicted by the colored boxes (legend on right). Top row of boxes corresponds to ground-based system point density, bottom row corresponds to airborne system.

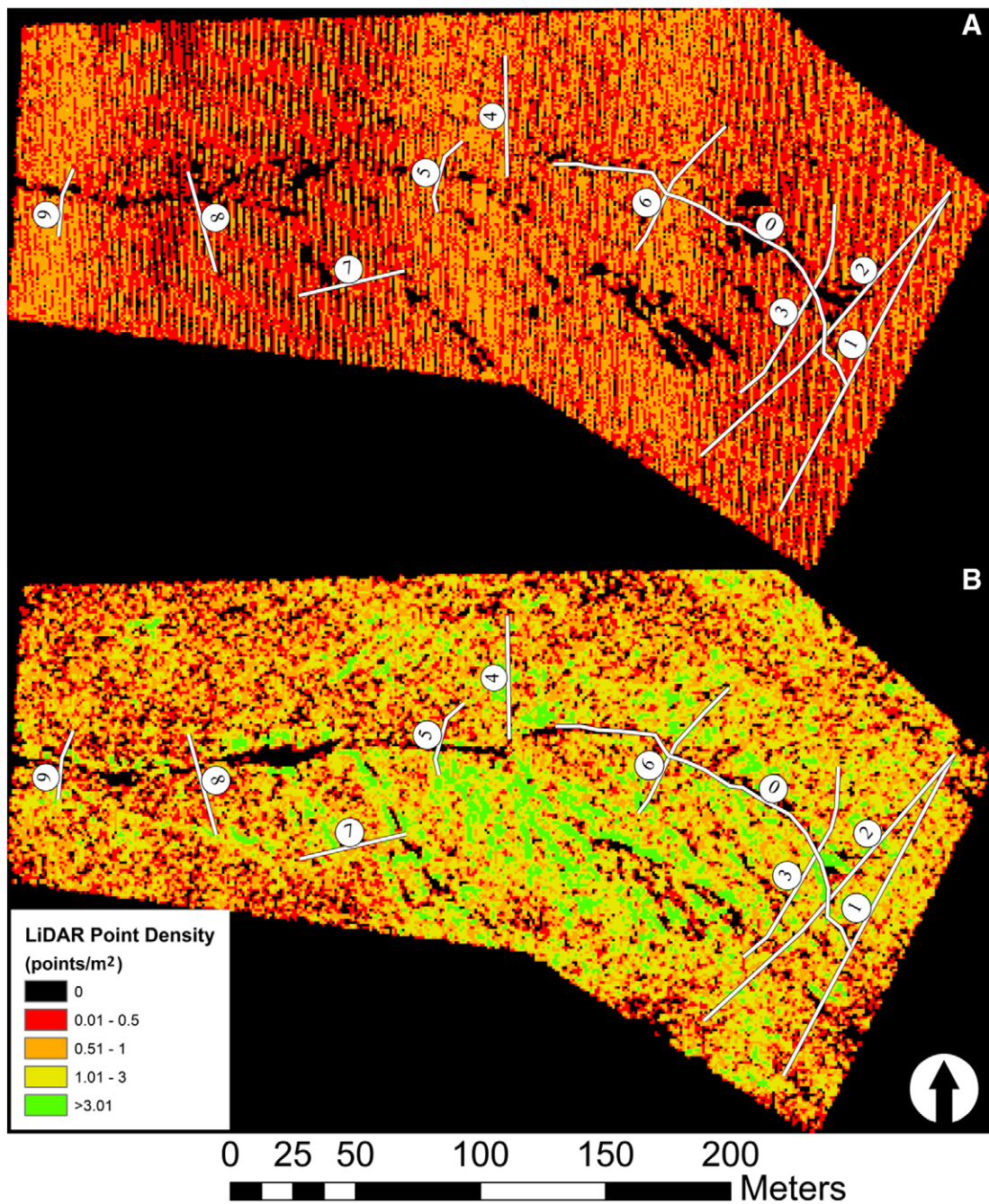


Fig. 8. Lidar point density of (A) airborne and (B) ground-based LiDAR systems over the study area. Total station transects are numbered and shown in white.

system (between the black and grey arrows), though there appears to be a crossover point of absolute elevation error (marked by a grey arrow) of ~0.70 m beyond which the airborne system is superior.

Table 2
LiDAR point density data for gullied and non-gullied areas.

Class	Avg. point density (points m ⁻²)	Max. point density (points m ⁻²)	% of zero returns
Airborne non-gullied area	0.3	1.6	14
Airborne gullied area	0.1	1.6	20
Airborne total station transects	0.4	1.3	17
Ground-based non-gullied area	0.8	18.1	9
Ground-based gullied area	0.5	20.1	12
Ground-based total station transects	1.3	8	14

4.3. Estimation of gully volumes by comparison of present-day and modeled pre-erosion DEMs

Airborne LiDAR-derived DEMs of the present-day surface and modeled pre-erosion surface were compared (Fig. 11) and their difference calculated, producing a raster image with cell values containing 'elevation-difference' values. The cells of that DEM were summed and then multiplied by the cell resolution squared (2.25 m²) to produce a volumetric estimate of the amount of soil lost via gully erosion. This amount was calculated to be 19,249 m³ for a gullied area of 25,323 m². Example topographic transects of both the airborne LiDAR-derived DEM and the modeled pre-erosion surface are shown in Fig. 12. Similar calculations were attempted for the ground-based LiDAR-derived DEMs, but data gaps in the ground-based coverage precluded analysis of the entire study area.

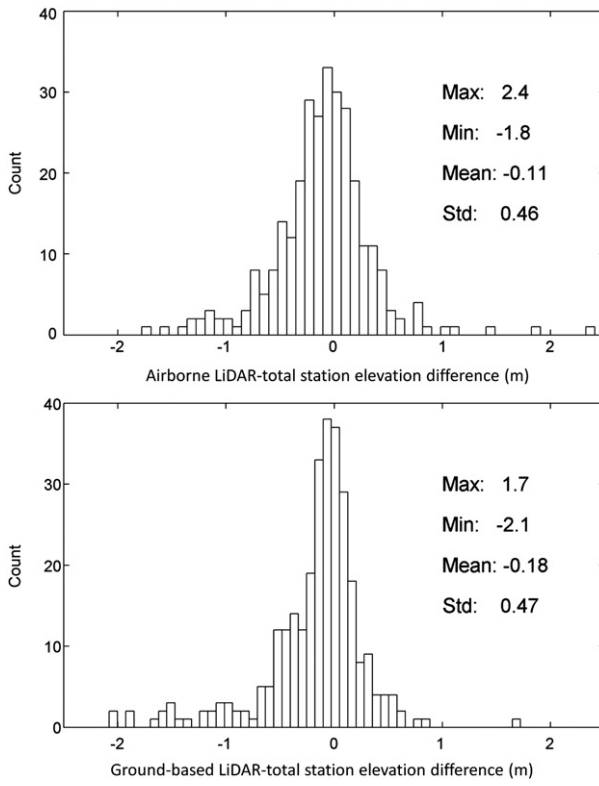


Fig. 9. Histograms of airborne and ground-based LiDAR vertical errors as measured from total station data. Both histograms are negatively skewed, showing the tendency to underestimate gully depths. Histograms have 50 bins, each ~ 0.085 m wide.

4.4. Alluvial fan volume estimation

The alluvial fan located at the foot of the study site acts as a transient storage zone for sediment leaving the catchment, presenting an opportunity to measure transient mass flux and storage as well as an indirect check on our volumetric erosion estimates. Interpolation of the hand-auger data collected over the alluvial fan immediately below the study area provided an estimate of historically deposited fan thickness (Fig. 13). As it was difficult to clearly identify the outer boundary of the alluvial fan in the field due to contributions from neighboring gully systems and losses due to lateral migration of the main channel arroyo, three different alternatives of alluvial fan extent were drawn and their volume calculated to give a range of possible sediment volumes stored within the fan. Delineation of the minimum

fan extent was based on the topographic envelope of the obvious alluvial surface, while the larger estimated fan boundaries include more distal deposits that may also contain sediment originating from further upstream. These volumes ranged from 6213 to 15,145 m³ and are all substantially less than the amount of material estimated to have been lost from the gully system directly above, suggesting that much of the sediment is not stored in this immediate alluvial fan. Using this range of alluvial fan volumes and our raw estimate of DEM-derived gully erosion, we calculate a net storage of 32–78% of eroded sediment in the alluvial fan. This lower storage estimate is supported by historic aerial imagery, which shows dynamic fan behavior and migration through time, including deposition of sediment much further down on the floodplain (Fig. 14).

5. Discussion

5.1. Comparison of airborne and ground-based LiDAR with total station data

Both LiDAR datasets underestimated the depth of gully features, with average cross-sectional errors of -5.2 m² (airborne) and -9.7 m² (ground-based). In order to produce a three-dimensional estimate of volumetric error, we assume that the total station transect data are representative of the entire gully system. In addition, we assume that volumetric error is strongly related to point density, and most importantly to those areas with zero point returns. Gullied areas had lower LiDAR point densities and a higher percentage of zero point returns than non-gullied areas (Table 2). As the total station transects and gullied areas both show a similar percentage of zero returns, we believe it is reasonable to extrapolate the cross-sectional errors into three dimensions, while recognizing that there are a limited number of transects.

Averaged over a distance of ~ 500 m (the approximate length of the study site gully network), volumetric underestimates were 2605 m³ for the airborne system and 4849 m³ for the ground-based system, or about 14% and 25% of the excavated material, respectively.

The most likely source of the errors in volume is laser point density and spacing. As shown in Fig. 8, the airborne system had an average point density well below 1.0 point m⁻². Although this density is more than adequate for measuring most topographic features, the shape and size of gullies presents unique challenges. The steep gully side walls and v-shaped cross-sections produce rapid elevation changes over short distances, and unless the laser directly strikes the gully axis, the resulting DEM will always underestimate gully depth and therefore incised volume. These issues exist in addition to more typical bare-earth LiDAR processing problems such as accurate vegetation removal.

We expected the ground-based LiDAR dataset to produce better gully volume estimates than the airborne data because it can produce much higher point densities. Indeed, if the position of the ground-based LiDAR allows observation of the entire gully, the data density and volume estimations should be equal to or better than the total station surveys. However, the side-looking orientation of the ground-based system meant that steep-sided, deep (>0.5 m) gully geometries created topographic shadows and greater error. Gully bottoms were often entirely obstructed from view with the ground-based system. With no data points within the area of interest, the interpolated DEM invariably produced a surface higher than the true gully elevation, as illustrated in Fig. 7, and especially the plot of transect 5, where the point density for the ground-based system within the main gully channel was zero. Due to time constraints in the field, it was not possible to collect measurements from enough different positions to adequately cover the most incised parts (lower reaches) of the study site (Fig. 2). We estimate that an additional two full days would have been needed to obtain complete coverage of the study area with the ground-based system, producing a more accurate dataset than that of the airborne LiDAR system. This estimate is based on the more than 30 hours of active scanning required to collect data from our existing 37 scan locations, working downstream from the upper reaches on foot in an effort to

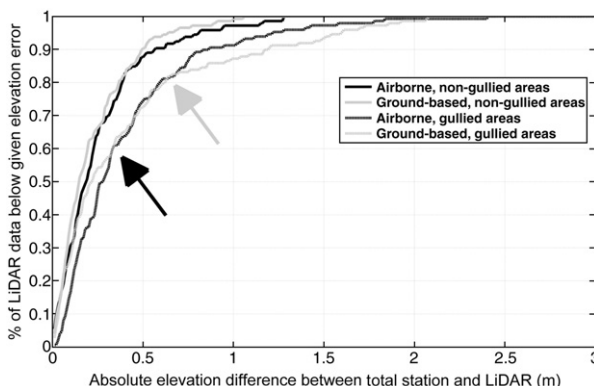


Fig. 10. Cumulative probability plot of absolute vertical errors for airborne (black) and ground-based (grey) LiDAR systems, segregated by non-gullied (solid) and gullied (dashed) areas. Black arrow indicates point below which ground-based system is superior for gullied areas. Grey arrow indicates point above which airborne system is superior for gullied areas.

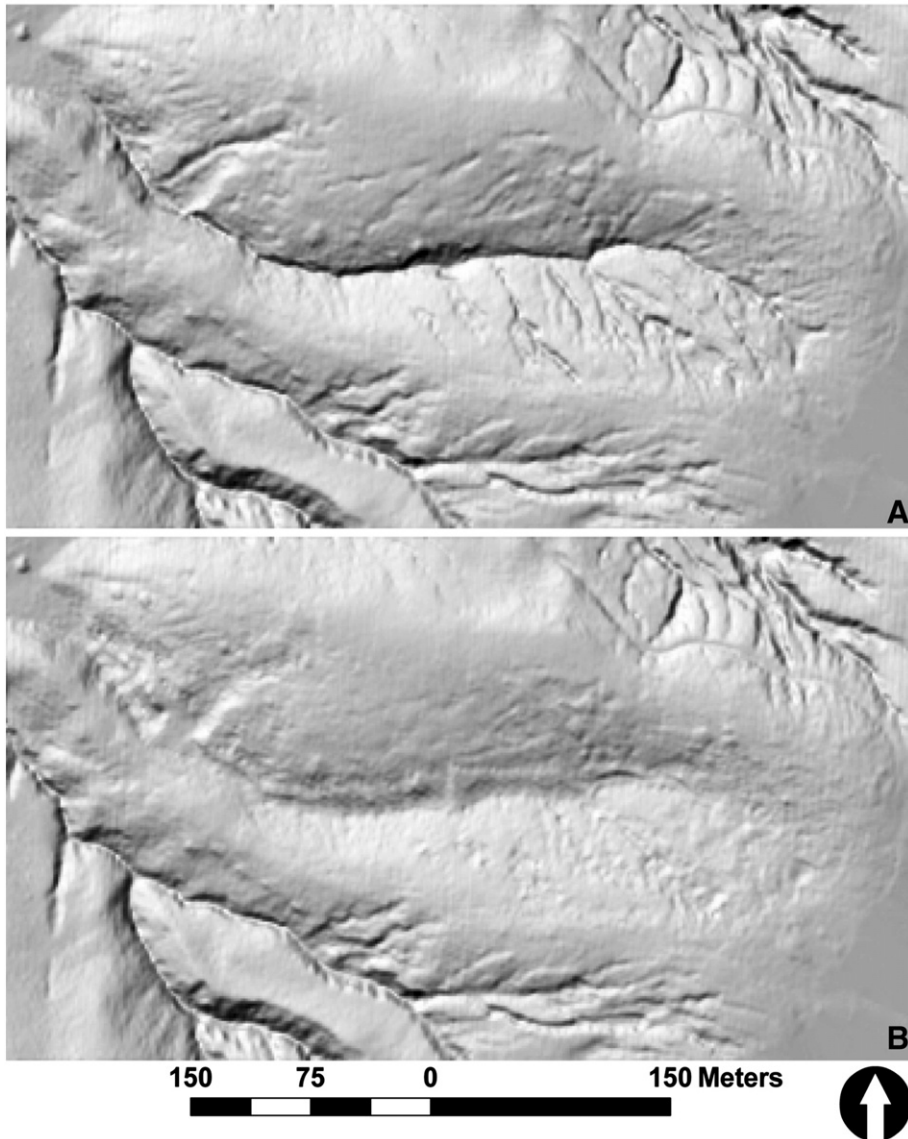


Fig. 11. Hillshade-relief images of present-day airborne LiDAR-derived DEM (A) and pre-erosion modeled surface (B). The volumetric difference between the two surfaces is 19,249 m³.

produce a catchment-averaged value. This suggests that for future studies characterizing deeply incised gullies in remote and rugged terrain with a ground-based LiDAR system, workers should allot roughly 1 day per 1.5×10^{-2} km² of scanned area. There is a marked difference in error between gullied and non-gullied areas for both the ground-based and airborne systems (Fig. 10). For non-gullied areas, the ground-based system always outperforms the airborne LiDAR because of its higher point density, and the absence of obstructing features. In gullied areas, the ground-based system either outperforms or does as well as the airborne system for ~83% of the coverage. But for the last 17% (above the grey arrow on Fig. 10), the cumulative error curve produced by data from the ground-based system flattens out and produces greater errors than the airborne system. This error pattern is especially pertinent in the deeply incised channels in the lower reaches of our study area. As seen in the inset photo of Fig. 2, the deepest portion of the gully at the thalweg is often where elevations change most rapidly, and missing this section from the dataset will produce large vertical errors in the resulting DEM.

To produce a more accurate survey of the incised channels using the ground-based LiDAR system, it would be necessary to get near-perfect view angles into the gullies. With unlimited time and resources for data collection, the ground-based LiDAR system has the potential to produce a highly accurate, 1- to 10-cm scale DEM of the study area. Nevertheless,

basic logistical issues associated with getting the instrument to the gully floor, and the restricted line of sight within the winding gullies, make that goal nearly unattainable. While the ground-based system has significant advantages over previous methods of gully erosion estimation, especially for the upper reaches where gully incision is not deep enough to produce significant topographic shadowing or inhibit instrument movement, its spatial coverage limitations are problematic. The best solution would seem to be a combination of higher resolution (decimeter point spacing) airborne LiDAR data across the study area to capture the main gully system, and ground-based LiDAR data of the upper reaches to capture the smaller gully tributaries.

Regardless, both systems can discriminate and measure gully features that are effectively invisible at existing coarser-resolution DEM datasets (e.g., National Elevation Dataset). In addition, corrections based on known sources of error as measured by total station or other instrumentation in the field can be applied to the LiDAR-derived erosion volume estimates to improve results. These results suggest that LiDAR datasets can be used to quantify gully erosion, but proper care must be taken. Without additional field data to verify and constrain DEM accuracy, LiDAR-derived products should not be accepted without question. Laser-spot spacing and landscape complexity, including the density of vegetation cover and sinuosity and steepness of gullying, must be taken into account when

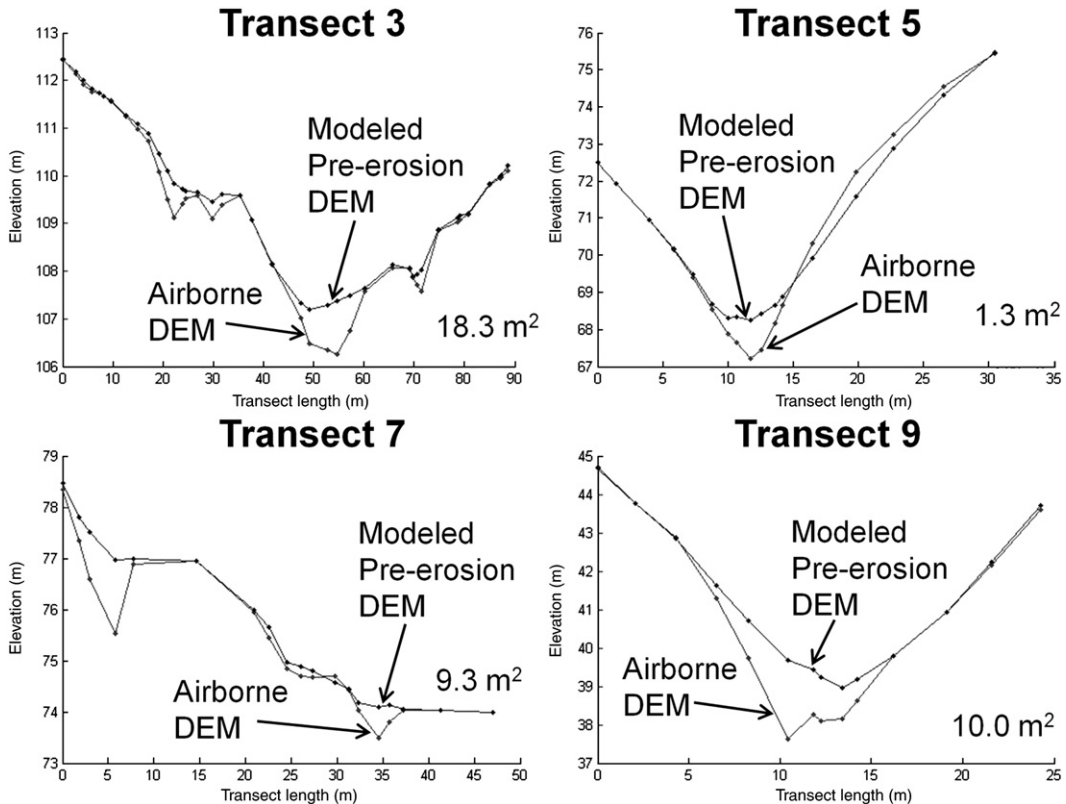


Fig. 12. Topographic profiles of four transects from the airborne LiDAR-derived DEM and modeled 'pre-erosion' DEM. Numbers indicate the estimated cross-sectional area of present gullies.

determining the amount of required field verification data. Given the overall better performance of the airborne system in gully volume quantification and greater spatial coverage, the remainder of the discussion will focus on the airborne system.

5.2. Modeled pre-erosion DEM

Often gullies develop in pre-existing topographic lows where water is concentrated. Therefore, it is important to distinguish between antecedent

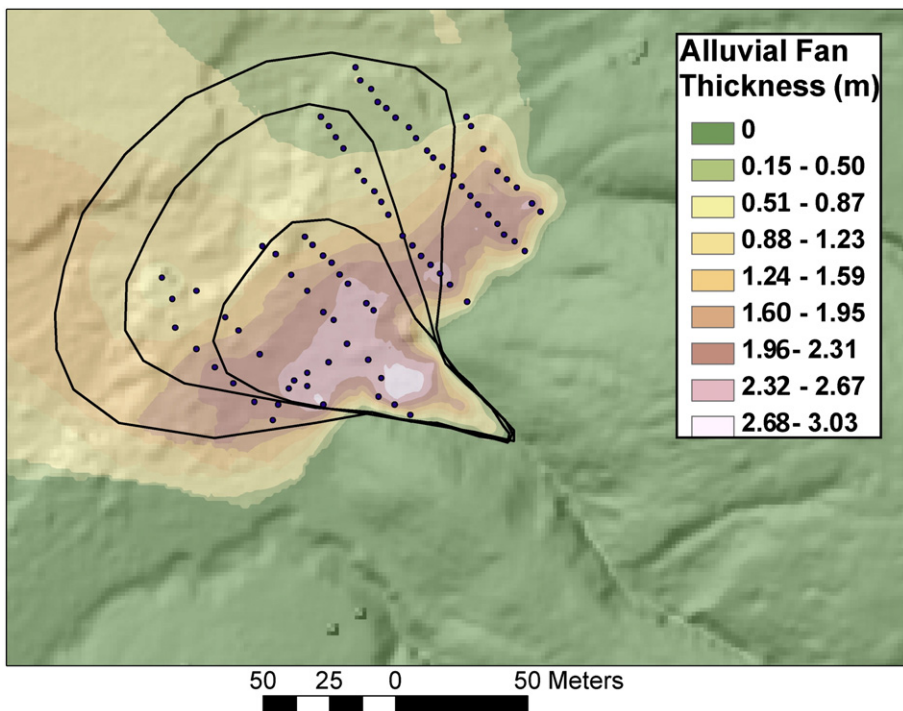


Fig. 13. Alluvial fan thickness as derived from interpolated hand-augur data (sample locations denoted by black circles). Fan volume estimates for small, medium, and large fan sizes are 6213 m^3 , 9828 m^3 , and $15,145 \text{ m}^3$ respectively.

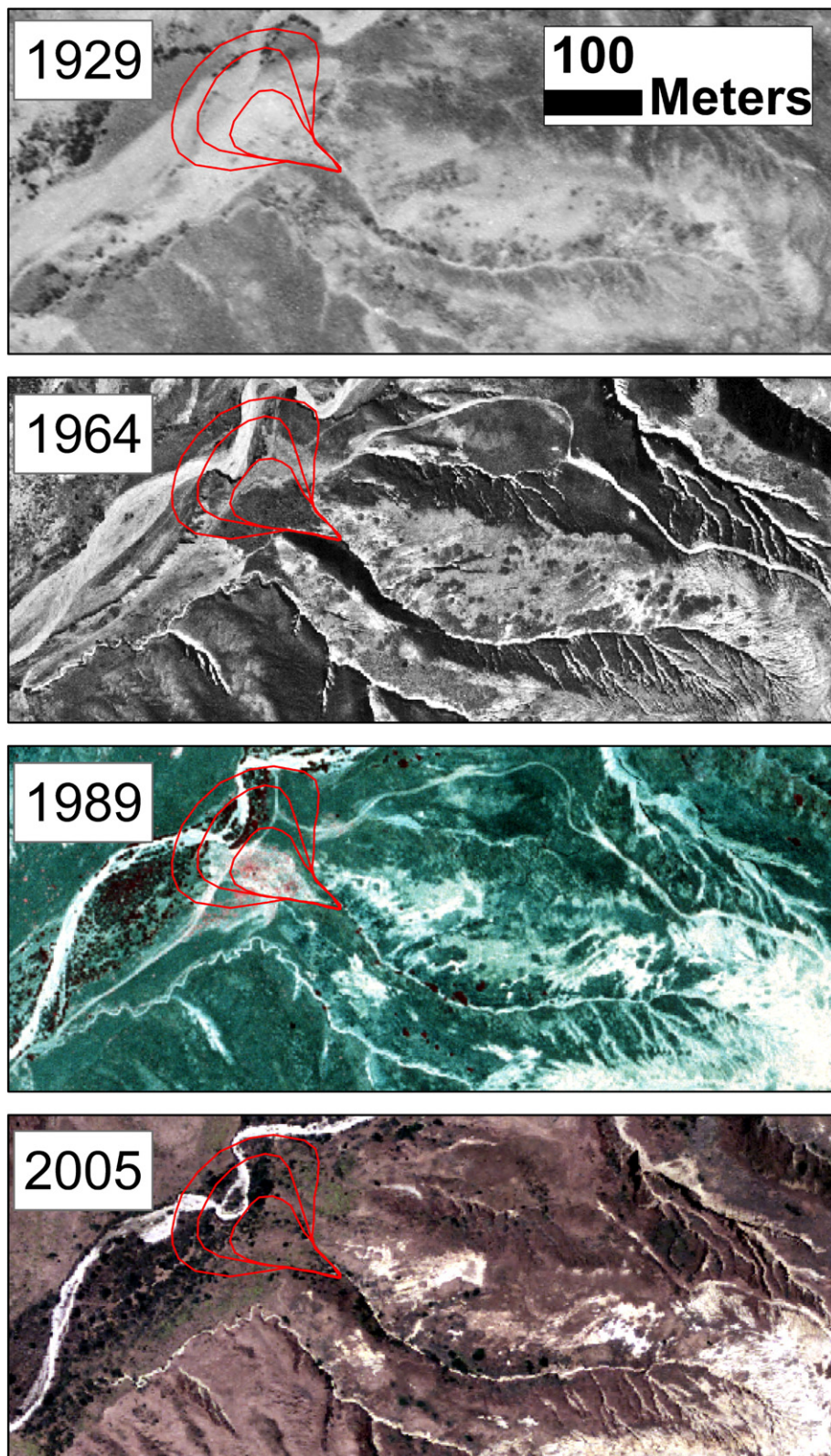


Fig. 14. Aerial imagery time-series showing migration of study site alluvial fan deposition through time. Light-colored areas are bare soil. Fan is inactive and covered by vegetation by 2005. Red lines show small, medium, and large alluvial fan size estimates from Fig. 13.

stream valleys and recently eroded gullies. While in many places re-creating the pre-existing topography is an obvious process (Fig. 12, Transect 7), in others, accurate re-creation of the pre-erosion surface can be more difficult (Fig. 12, Transect 9). Capturing the subtle slope

relationships that exist where there are gullies within valleys required field observation and manual modification of delineation processes. It is unlikely that this process can be circumvented unless the landscape is quite simple (i.e. gullies in a planar surface).

5.3. Gully erosion volume estimate

We used the total station data to optimize the volume estimate mass loss from gullies using the airborne LiDAR data. The original estimate ($19,249 \text{ m}^3$) plus the underestimation error (2605 m^3), results in $21,854 \text{ m}^3$ of material lost over a gullied area of $25,323 \text{ m}^2$, or $0.86 \text{ m}^3 \text{ m}^{-2}$. Recent work on estimating gully erosion volumes from active gullies in the black soil region of northeastern China (0.86 to $2.24 \text{ m}^3 \text{ m}^{-2}$) and the Guadalestín Basin in Southeast Spain ($2.11 \text{ m}^3 \text{ m}^{-2}$), are at the low end of these results (Wu et al., 2008; Marzolff and Poesen, 2009).

5.4. Alluvial fan: mass transfer and storage of eroded sediment

Hand-auger measurements indicate that 28–70% of the estimated sediment eroded from the gully system is currently stored on the alluvial fan at the base of the study site, with the remainder either deposited further down the floodplain or lost out to sea. The historic aerial photo record shows impressive fan migration through time, with active deposition varying substantially across the floodplain over a 60-year period (Fig. 14). Both of these independent observations suggest that our LiDAR-derived gully erosion volume estimate is reasonable.

5.5. Expansion of results to southwestern SCI

The gully erosion of the study site is typical for areas underlain by the Tertiary sedimentary formations of southwestern SCI. In fact, it is virtually impossible to find an un-gullied catchment in this part of the island. Taking the findings ($21,854 \text{ m}^3$ lost over a catchment area of $7.546 \times 10^{-2} \text{ km}^2$, or $0.29 \text{ m}^3 \text{ m}^{-2}$) as representative of gully erosion occurring over all Tertiary sedimentary units on southwestern SCI (13.502 km^2), we estimate that there has been $3.91 \times 10^6 \text{ m}^3$ of material lost as a result of gully erosion. Much of this material is derived from upper organic-rich A horizons, exposing nutrient-poor subsoil that has hindered vegetation recovery processes. Historic gully erosion on SCI has dramatically redistributed large amounts of sediment across the landscape over a relatively brief period, with fundamental geomorphic and ecological implications.

6. Conclusion

LiDAR based datasets support quantifiable landscape-level estimates of gully erosion that were previously impossible without highly labor- and time-intensive field measurements. These volume estimates can be used to better understand geomorphic processes and to quantify erosion losses for land management decisions. Both airborne and ground-based LiDAR datasets underestimated gully erosion volumes. Errors can be minimized by using higher resolution (decimeter point spacing) airborne data and manual optimization using field data. The method used to recreate the pre-erosion surface provides a reasonable first attempt but would greatly benefit from future refinement and automation. The limited footprint and side-looking orientation of the ground-based LiDAR system presented difficulties given limited time and resources, but it could be more useful if data were collected from more view angles. Furthermore, the ground-based system would be very useful in developing relatively low-cost time-series data sets to monitor the severity of ongoing gully erosion processes.

Acknowledgements

The authors would like to thank The Nature Conservancy and the University of California Natural Reserve System, specifically Lyndal Laughrin, for access to southwestern Santa Cruz Island; Mike Kambitsch at Pacific Western Aerial Surveys and the UCSB Map and

Imagery Laboratory for access to historic aerial imagery, and the following people for assistance in the field: Caroline Guebels, Billy Doles, James Worthington, Hendrik Wulf, Mark Collar, Katherine Lindburgh, Park Williams, Jeff Howarth and Carl Legleiter. The research described in this paper has been funded wholly or in part by the United States Environmental Protection Agency (EPA) under the Science to Achieve Results (STAR) Graduate Fellowship Program. The EPA has not officially endorsed this publication and the views expressed herein may not reflect the views of the EPA.

References

- Asner, G.P., Knapp, D.E., Jones, M.O., Kennedy-Bowdoin, T., Martin, R.E., Boardman, J., Field, C.B., 2007. Carnegie Airborne Observatory: in-flight fusion of hyperspectral imaging and waveform light detection and ranging (wLiDAR) for three-dimensional studies of ecosystems. *J. Appl. Rem. Sens.* 1, 013536.
- Asner, G.P., Hughes, R.F., Vitousek, P.M., 2008. Invasive plants transform the three-dimensional structure of rain forests. *Proc. Nat. Acad. Sci.* 105, 4519–4523.
- Ayoub, F., Leprince, S., Avouac, J.P., 2009. Co-registration and correlation of aerial photographs for ground deformation measurements. *ISPRS J. Photogram. Rem. Sens.* 64, 551–560.
- Betts, H.D., DeRose, R.C., 1999. Digital elevation models as a tool for monitoring and measuring gully erosion. *Int. J. App. Earth Obs. and Geoinf.* 1, 91–101.
- Brumbaugh, R., 1983. Hillslope gullyling and related changes, Santa Cruz Island, California. Ph.D. Thesis, UCLA, Los Angeles, California.
- Casalí, J., Loizu, J., Campo, M.A., De Santisteban, L.M., Álvarez-Mozos, J., 2006. Accuracy of methods for field assessment of rill and ephemeral gully erosion. *Catena* 67, 128–138.
- Chaplot, V., Giboire, G., Marchand, P., Valentin, C., 2005. Dynamic modelling for linear erosion initiation and development under climate and land-use changes in northern Laos. *Catena* 63, 318–328.
- Collins, B.D., Kayen, R., 2006. Applicability of Terrestrial LiDAR Scanning for Scientific Studies in Grand Canyon National Park, Arizona: U.S. Geological Survey, Open-File Report 2006-1198.
- Collins, B.D., Brown, K.B., Fairley, H.C., 2008. Evaluation of terrestrial LiDAR for monitoring geomorphic change at archeological sites in Grand Canyon National Park, Arizona. U.S. Geological Survey Open-File Report 2008-1384.
- Collins, B.D., Minasian, D., Kayen, R., 2009. Topographic Change Detection at Select Archeological Sites in Grand Canyon National Park, Arizona, 2006–2007. U.S. Geological Survey Scientific Investigations Report 2009-5116.
- Costa, F.M., Bacellar, Lde. Almeida Prado, 2007. Analysis of the influence of gully erosion in the flow pattern of catchment streams, Southeastern Brazil. *Catena* 69, 230–238.
- De Vente, J., Poesen, J., Verstraeten, G., 2005. The application of semi-quantitative methods and reservoir sedimentation rates for the prediction of basin sediment yield in Spain. *J. of Hyd.* 305, 63–86.
- Eustace, A., Pringle, M., Witte, C., 2009. Give me the dirt: detection of gully extent and volume using high-resolution lidar. In: Jones, S., Reinke, K. (Eds.), *Innovations in Remote Sensing and Photogrammetry*. Springer-Verlag, Berlin Heidelberg, pp. 255–269.
- Glenn, N.F., Streutker, D.R., Chadwick, D.J., Tahckray, G.D., Dorsch, S.J., 2006. Analysis of LiDAR-derived topography information for characterizing and differentiating landslide morphology and activity. *Geomorphology* 73, 131–148.
- Hancock, G.R., Crawter, D., Fityus, S.G., Chandler, J., Wells, T., 2008. The measurement and modelling of rill erosion at angle of repose slopes in mine spoil. *Earth Surf. Process. Landf.* 33, 1006–1020.
- Heritage, G.L., Hetherington, D., 2007. Towards a protocol for laser scanning in fluvial geomorphology. *Earth Surf. Process. Landf.* 32, 66–74.
- Horton, R.E., 1945. Erosional development of streams and their drainage basins: hydrophysical approach to quantitative morphology. *Geol. Soc. Am. Bull.* 56, 275–370.
- Huon, S., Bellanger, B., Bonte', Ph., Podwojewski, P., Valentin, C., Velasquez, F., Bricquet, J.-P., de Rouw, A., Girardin, C., 2005. Monitoring soil organic carbon erosion with isotopic tracers, two case studies on cultivated tropical catchments with steep slopes (Laos, Venezuela). : Advances in Soil Science. CRC Press, Boca Raton, Florida, USA.
- Ireland, H.A., Sharpe, C.F.S., Eargle, D.H., 1939. Principles of gully erosion in the Piedmont of South Carolina. U.S. Dept. of Ag. Tech. Bul. 633, 142.
- James, L.A., Watson, D.G., Hansen, W.F., 2007. Using LiDAR data to map gullies and headwater streams under forest canopy: South Carolina, USA. *Catena* 71, 132–144.
- Junak, S., Ayers, T., Scott, R., Wilken, D., Young, D., 1995. A Flora of Santa Cruz Island. Santa Barbara Botanic Garden, Santa Barbara, California.
- Kelsey, H.M., 1980. A sediment budget and an analysis of geomorphic process in the Van Duzen River basin, north coastal California, 1941–1975: summary. *Geol. Soc. Am. Bull.* 91, 190–195.
- Lawler, D.M., 1993. The measurement of river bank erosion and lateral channel change: a review. *Earth Surf. Process. Landf.* 18, 777–821.
- Leprince, S., Barbot, S., Ayoub, F., Avouac, J.P., 2007. Automatic and precise orthorectification, coregistration, and subpixel correlation of satellite images, application to ground deformation measurements. *IEEE Trans. Geosci. Rem. Sens.* 45, 1529–1558.
- Martinez-Casanovas, J.A., 2003. A spatial information technology approach for the mapping and quantification of gully erosion. *Catena* 50, 293–308.

- Martinez-Casanovas, J.A., Ramos, M.C., Poesen, J., 2004. Assessment in sidewall erosion in large gullies using multi-temporal DEMs and logistic regression analysis. *Geomorphology* 58, 305–321.
- Marzolff, I., Poesen, J., 2009. The potential of 3D gully monitoring with GIS using high-resolution aerial photography and a digital photogrammetry system. *Geomorphology* 111, 48–60.
- McKean, J., Roering, J., 2004. Objective landslide detection and surface morphology mapping using high-resolution airborne laser altimetry. *Geomorphology* 57, 331–351.
- Milan, D.J., Heritage, G.L., Hetherington, D., 2007. Applications of a 3D laser scanner in the assessment of erosion and deposition volumes and channel change in a proglacial river. *Earth Surf. Process. Landf.* 32, 1657–1674.
- Moody, J.A., Kinney, D.A., 2006. Spatial structures of stream and hillslope drainage networks following gully erosion after wildfire. *Earth Surf. Process. Landf.* 31, 319–337.
- Nearing, M.A., Pruski, F.F., O'Neal, M.R., 2004. Expected climate change impacts on soil erosion rates: a review. *J. Soil Water Cons.* 59, 43–50.
- Nunes, J.P., Seixas, J., Pacheco, N.R., 2008. Vulnerability of water resources, vegetation productivity and soil erosion to climate change in Mediterranean watersheds. *Hyd. Process.* 22, 3115–3134.
- Nunes, J.P., Seixas, J., Keizer, J.J., Ferreira, A.J.D., 2009. Sensitivity of runoff and soil erosion to climate change in two Mediterranean watersheds. Part II: assessing impacts from changes in storm rainfall, soil moisture and vegetation cover. *Hyd. Process.* 23, 1212–1220.
- Nyssen, J., Poesen, J., Veyret-Picot, M., Moeyersons, J., Mitiku, H., Deckers, J., Dewit, J., Naudts, J., Kassa, T., Govers, G., 2006. Assessment of gully erosion rates through interviews and measurements: a case study from Northern Ethiopia. *Earth Surf. Process. Landf.* 31, 167–185.
- Perroy, R.L., 2009. Quantifying land degradation and vegetation recovery on southwestern Santa Cruz Island, California. Ph.D. Thesis. UCSB, Santa Barbara, California.
- Poesen, J., Nachtergale, J., Vertstraeten, G., Valentin, C., 2003. Gully erosion and environmental change. Importance and research needs. *Catena* 50, 91–134.
- Rosser, N.J., Petley, D.N., Lim, M., Dunning, S.A., Allison, R.J., 2005. Terrestrial laser scanning for monitoring the process of hard rock coastal cliff erosion. *Q. J. Eng. Geol. Hydrogeol.* 38, 363–375.
- Rustomji, P., 2006. Analysis of gully dimensions and sediment texture from southeast Australia for catchment sediment budgeting. *Catena* 67, 119–127.
- Soil Science Society of America, 2001. Glossary of Soil Science Terms. Soil Science Society of America, Madison, WI, <http://www.soils.org/ssagloss/>.
- Strahler, A.N., 1952. Hypsometric (area-altitude) analysis of erosional topography. *Geol. Soc. Am. Bull.* 63, 1117–1142.
- Thoma, D.P., Gupta, S.C., Bauer, M.E., Kirchoff, C.E., 2005. Airborne laser scanning for riverbank erosion assessment. *Rem. Sens. Env.* 95, 493–501.
- Valentin, C., Poesen, J., Yong, L., 2005. Gully erosion: impacts, factors and control. *Catena* 63, 132–153.
- Vosselman, G., Maas, H., 2001. Adjustment and filtering of raw laser altimetry data. *Proc. OEEPE workshop on Airborne Laserscanning and Interferometric SAR for Detailed Digital Elevation Models*, OEEPE Pub. 40, Stockholm, Sweden.
- Wasson, R.J., Caitcheon, G., Murray, A.S., McCulloch, M., Quade, J., 2002. Sourcing sediment using multiple tracers in the catchment of Lake Argyle, northwestern Australia. *Env. Manag.* 29, 634–646.
- Wawrzyniec, T.F., McFadden, L.D., Ellwein, A., Meyer, G.A., Scuderi, L., McAuliffe, J., Fawcett, P., 2007. Chronotopographic analysis directly from point cloud data: a method for detecting small, seasonal hillslope change, Black Mesa escarpment, NE Arizona. *Geosphere* 3, 550–567.
- Wells, R.R., Alonso, C.V., Bennett, S.J., 2009. Morphodynamics of headcut development and soil erosion in upland concentrated flows. *Soil Sci. Soc. Am. J.* 73, 521–530.
- Wu, Y., Zheng, Y., Zhang, Y., Liu, B., Cheng, H., Wang, Y., 2008. Development of gullies and sediment production in the black soil region of northeastern China. *Geomorphology* 101, 683–691.
- Young, A.P., Ashford, S.A., 2006. Application of airborne LIDAR for seafloor volumetric change and beach-sediment budget contributions. *J. Coast. Res.* 22, 307–318.